General introduction

Photosynthesis has been attracted many scientists due to its importance for biological systems and general interests in the mechanism of transformation of a photo-activation energy into a chemical energy source. Two processes, a light reaction and a dark reaction, are found in nature. The former process consists of Photosystem I and II, some electron transfer molecules such as a plastocyanin, $NADP^+$ reductase, and so on. In the latter system, A CO_2 fixing enzyme, ribulose-1,5-bisphosphate carboxylase/ oxygenase (RuBisCO), plays the most important role in the Calvin cycle with NADPH and ATP yielded from the light reaction.

The photo-activation in the light reaction has been found in only the biological systems with light-harvesting complexes. Recently, a novel photo-activation system with a chromoprotein, has found in a mushroom, *Pleurotus salmoneostramineus* L. Vass..

In the dark reaction, the CO_2-fixing process catalyzed by RuBisCO is the rate-determining step. This enzyme has much slower rate than other enzymes, although it is crucial for the crop yields and maintaining the CO_2 concentration in air.

In this study, I report the structural analyses on chromoprotein, plastocyanin, and RuBisCO to clarify their function and to resolve the current global problems.

1 Novel insight into the structure-function relationship of the proteins involved in light reaction

1.1 Chromoprotein from *Pleurotus salmoneostramineus*

1.1.1 Properties of chromoprotein *Pleurotus salmoneostramineus* L. Vass.

Pleurotus salmoneostramineus L. Vass., a kind of mushroom found in Siberia, Japan and New Guinea, is known for its beautiful pink color. This mushroom includes a pink chromoprotein with an absorption spectrum maximum at 496 nm. This protein has a pigment molecule, 3*H*-indol-3-one (indolone), which occupies a part of the active site (Takekuma *et al.*, 1994) and has three kinds of metals, Zn, Fe, and Cu. Indolone has an absorption maximum at 456 nm in methanol and bathochromic shift occurs in the chromoprotein. Takekuma *et al.* have reported that the protein produces oxygen molecules from water on light irradiation. This phenomenon implies that this mushroom has a photosynthetic function in which the chromoprotein plays an important role (Takekuma *et al.*, 1994). The aim of the present study is to reveal the structure-function relationship of the chromoprotein with the novel photosynthetic mechanism.

1.1.2 Purification and crystallization of chromoprotein

Chromoprotein was extracted by soaking the mushrooms in water. Crude chromoprotein was freeze-dried and stored at -78 ˚C. The protein (0.5 g) was dissolved in 1 ml of Tris-HCl buffer (pH 7.0), then applied onto a Sephacryl S-300HR column (Pharmacia, 3 × 80 cm, pre-equilibrated in Tris-HCl buffer, pH 7.0). The fractions containing the chromoprotein were collected and dialyzed for 12 h against glycine-NaOH buffer (pH 10.0). It was loaded on DEAE-Sepharose column (2 × 30 cm) equilibrated in glycine-NaOH buffer (pH 10.0) and then washed with 20 mM NaCl solution in the elution buffer. The purified protein was dialyzed against water and concentrated up to 10 Abs/cm at 496 nm.

Single crystals were obtained by vapor diffusion method. The reservoir consists of 50 mM buffer solution (Tris-HCl, pH 9.0) containing 21% (w/v) polyethylene glycol 4600 and 200 mM sodium formate. The protein drop was prepared by mixing 3μl of protein solution with 3μl of reservoir solution. Single red-colored crystals appeared as prismatic needles within one week (Fig. 1).

1.1.3 X-ray analysis of chromoprotein

Preliminary X-ray experiments were carried out on a Rigaku R-AXIS IIC imaging plate detector system equipped with a Rigaku RU-300 rotating-anode X-ray generator (fine-focused Cu$K\alpha$, operating at 40 kV and 100 mA). The Laue symmetry and cell dimensions were determined by *PROCESS* program package (Higashi, 1989; Sato *et al.*, 1992) and systematic absences were confirmed by pseudo-precession pictures using the program *HKLPLOT* (Eleanor Dodson, unpublished data; Collaborative Computational Project, Number 4, 1994). The crystals belong to monoclinic space group *C*2 with the unit cell dimensions of a = 118.5, b = 59.7, c = 31.8 Å and β = 114°. Supposing one molecule per asymmetric unit, *Vm* value is calculated to be 2.1 Å^3/Da. (Matthews, 1968). Diffraction was found on imaging plates up to 2.5 Å resolution.

Diffraction intensity data for a native crystal were collected by using synchrotron radiation (BL-18B beam line, Photon Factory, KEK, Japan). The Weissenberg camera for macromolecules (Sakabe, 1991) and large imaging plates (40 × 80 cm) were used for data collection. The crystal diffracts up to 1.8 Å resolution and 15 frames with a rotation angle of 12.5° for each frame were stored. During the data collection no obvious radiation damage was detected. Data processing was carried out by the program *DENZO* and *SCALEPACK* (Otwinowski, 1993). The combined set gave 71,241 reflections to 1.8 Å resolution in total, which were reduced 18,198 unique reflections with an R_{merge} of 4.8% ($R_{merge} = \Sigma|I - \langle I \rangle|/\Sigma I$) and the completeness of 85.7% (61.4% for 1.80-1.86 Å) (Table I).

1.1.4 Structure analysis of chromoprotein

Structural analysis of chromoprotein is attempted by the isomorphous replacement method. Heavy atom derivatives are prepared by soaking the crystals into heavy metal solutions.

Two derivatives, $HgCl_2$ and CH_3HgCl, are successfully prepared. The statistics for both derivatives are summarised in Table I. Difference Patterson maps for both derivatives indicate that the heavy atom positions of a major site are the same (u=0.85, v=0.0, w=0.18) (Fig. 1 *a* & *b*). A monor site is found at u=0.4, v=0.25 w=0.45 only for the CH_3HgCl derivative (Fig. 1 *b* & *c*).

The refinements of the heavy atom position and phase calculations by the multiple isomorphous replacement (MIR) method with anomalous scattering of mercury ion were carried out by using the program *MLPHARE* in the *CCP4* suite (Otwinowski, unpublished program; Collaborative Computational Project, Number 4, 1994). Table II represents the results of the calculations. An MIR electron density map at 6 Å resolution clearly shown the dimensions and a shape of the molecule. Solvent flattening and histogram mapping methods were carried out by using the program *DM* (Cowtan, 1994; Collaborative Computational Project, Number 4, 1994). Solvent flipping and density truncation (also called "Solomon mode") were also applied with *DM*. Electron density maps for both strategies clealy represent the α-helices (Fig. 2). The chromoprotein has the dimensions of approximate 70 Å in length and 30 Å in width. At least, six α-helices were found in chromoprotein, one of them were quite long with approximate 40 residues (Fig. 3). The active site may be in the cavity surrounded by these α-helices. It is difficult to determine the structure of the active site with current

electron density map. Phase combination with current partial structure may be usuful for improvement of the phases.

Fig. 1 Crystals of chromoprotein. Dimensions of the largest crystal are 1.0 ∴ 0.07 ∴ 0.05 mm.

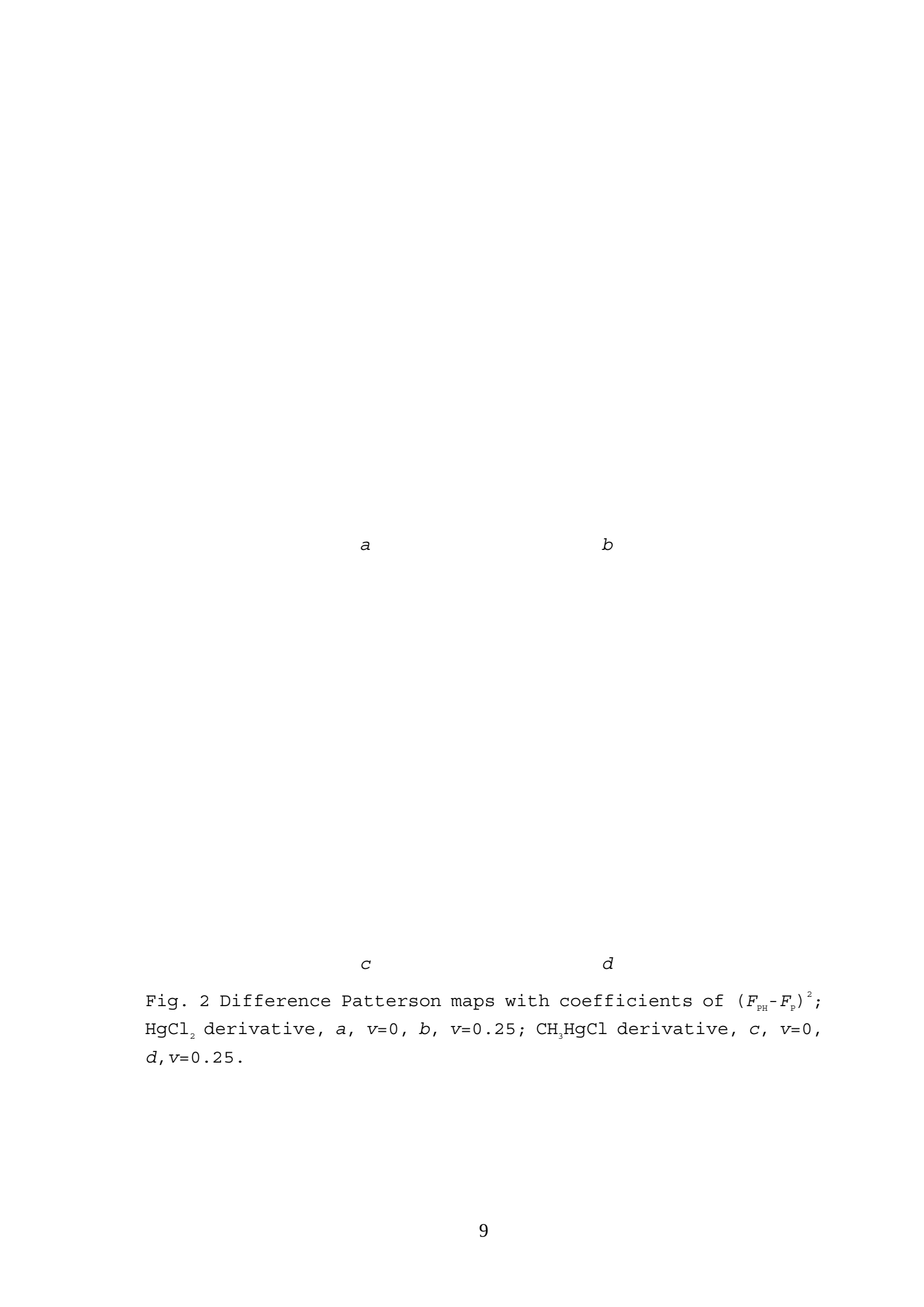

Fig. 2 Difference Patterson maps with coefficients of $(F_{PH}-F_P)^2$; $HgCl_2$ derivative, *a*, *v*=0, *b*, *v*=0.25; CH_3HgCl derivative, *c*, *v*=0, *d*, *v*=0.25.

Fig.3 Electron density maps of chromoprotein at 2.8 Å resolution after density modification with solvent flattening and histogram mapping (*a* and *c*), and with solvent flipping and density truncation (*b* and *d*)

Fig. 4 Stereo representation of partial structure of chromoprotein

1.2 Novel insight into the copper-ligands geometry and the electron transfer properties of blue-copper protein

1.2.1 Properties of plastocyanin

Plastocyanin is the key metalloprotein in the electron transfer processes from Photosystem II to Photosystem I. Plastocyanin consists of a polypeptide of approximate 100 amino acid residues and a type 1 copper atom (also called the "blue copper site") coordinated by side chains of four residues, two histidines, a cysteine, and a methionine. Plastocyanin has two electron transfer paths. One is the hydrophobic patch consists of hydrophobic residues at the northern end of the molecule (reviewed by Redinbo *et al.*, 1994) and the electron transfer occurs through His87. Another site is called negative patch or acidic patch located at the east end of the molecule and has Tyr83 as one of the electron paths, called a remote site, to the copper atom.

Crystal structure analyses of oxidized plastocyanins from poplar (Colman *et al.*, 1978; Guss *et al.*, 1992), green alga *Enteromorpha prolifera* (Collyer *et al.*, 1990) and *Chlamydomonas reinhardtii* (Redinbo *et al.*, 1993), have been carried out by X-ray crystallography, and NMR structures of reduced plastocyanin from french bean (Moore *et al.*, 1991), parsley (Bagby *et al.*, 1994) and blue-green alga *Anabaena variabilis* (Badsberg *et al.*, 1996) have been reported. Poplar plastocyanin is structurally best characterized by X-ray crystallography: structural studies on Hg(II)-substituted plastocyanin (Church *et al.*, 1986), and reduced plastocyanin at various pH are reported (Guss *et al.*, 1986).

At the active site, side chain atoms of the four residues,

hystidinyl nitrogens of His37 and His87, a cysteinyl sulfur of Cys84, and a methioninyl sulfur of Met92 coordinate to copper atom with a distorted tetrahedral geometry. In the oxidized condition, the bond lengths from Cu(II) to these ligands are approximate 1.9-2.2 Å except for Cu(II)-S_δ(Met92) bond of 2.8-2.9 Å. Pseudoazurin, one of the blue copper protein, has similar coordinational structure to plastocyanin. The bond distances from copper to two histidines and a cysteine are close to those of plastocyanin and the distance from copper to methioninyl sulfur is shorter by 0.1-0.2 Å.

The strong "blue" band near 600 nm corresponds to the intensed low-energy charge transfer from the S_γ(Cys) π-orbital to the Cu $d_{x^2-y^2}$ orbital which is the half-occupied redox-active HOMO (Solomon & Lowerly, 1993). The Cu $d_{x^2-y^2}$ orbital lies in the NNS plane (Louis *et al.*, 1996) formed by the two hystidinyl N_δ atoms and the cysteinyl S_γ atom, and the Cu-S_γ(Cys) bond bisects the lobes of the orbital (Solomon & Lowerly, 1993; Louis *et al.*, 1996). Recent studies on the electronic structure of nitrite reductase reported by Solomon and his co-workers indicate that the HOMO rotation relative to plastocyanin in the NNS plane decreases the intensity of the blue band (Louis *et al.*, 1996). Moreover, the geometry of the copper-thiolate bond will strongly influence the reduction potential and the electron transfer rates through the remote site.

The coordination geometry influences the EPR spectrum of blue copper protein. Plastocyanin shows axial EPR signal, whereas pseudoazurin shows rhombic one. It has been considered that the difference in the EPR spectrum is due to the stronger axial coordination in pseudoazurin (Kohzuma *et al.*, 1995). These results are consistent with the recent spectroscopic studies on nitrate

reductase and the different spectroscopic properties between plastocyanin and nitrite reductase are resulted from the different coordination geometry of sulfur atoms of cysteine and methionine at the copper site (Louis *et al.*, 1996).

Two hypotheses, the entatic state theory (Vallee & Williams, 1968; Williams, 1995) and the induced-rack theory (Gray & Malmström, 1983; Malmström, 1994), have been reported in metalloproteins. These theories are based on the idea that the copper-ligand geometry is strained by protein conformation. Recently, important studies on the copper-ligand coordination were carried out by Ryde *et al.* (1996). They calculated the optimized copper geometry on the modeled blue copper proteins and concluded that the results do not support these two hypotheses. Thus copper-ligands geometry is quite important for the functions and the spectroscopic properties of blue copper proteins. In the present work we report a novel insight into the structure of copper site.

1.2.2 Crystallization of *Ulva pertusa* plastocyanin

Single crystals of *U. pertusa* plastocyanin were obtained by vapor diffusion method. The reservoir solution consists of 100 mM buffer solution (pH 7.6) containing 2.2 M ammonium sulfate. The protein drop was prepared by mixing 3μl of protein solution (10 mg/ml) with 3μl of reservoir solution. Single cubic crystals appeared within one week (Fig. 5).

1.2.3 X-ray analyses and data Collection

Preliminary X-ray experiments were carried out on a Rigaku R-AXIS IIC imaging plate detector system equipped with a Rigaku RU-300 rotating-anode X-ray generator (fine-focused Cu$K\alpha$, operating at 40 kV and 100 mA). The Laue symmetry and cell dimensions were determined by the *PROCESS* program package (Sato *et al.*, 1992) and systematic absences were confirmed by pseudo-precession pictures using the program *HKLPLOT* (Collaborative Computational Project, Number 4, 1994). The crystal belongs to cubic space group $P4_132$ or $P4_332$ with the unit cell dimension of a = 88.3 Å. Supposing one molecule per asymmetric unit, Vm value is calculated to be 2.73 Å^3/Da (Solvent content 54.9%) (Matthews, 1968). Diffraction spots were found on imaging plates up to 2.0 Å resolution.

Diffraction intensity data were collected by using synchrotron radiation (BL-6B beam line, Photon Factory, KEK, Japan). The Weissenberg camera for macromolecules (Sakabe, 1991) and large imaging plates (40 × 80 cm) were used for the data collection. The crystal diffracts up to 1.6 Å resolution and 15 frames with a rotation angle of 2.5° for each frame were stored. During the data collection no obvious radiation damage was detected.

Data processing was carried out by the program *DENZO* and *SCALEPACK* (Otwinowski, 1993). The combined set gave 115,971 reflections to 1.6 Å resolution in total, which were reduced 14,759 unique reflections with the R_{merge} of 8.2% and the completeness of 91.5% (70.2% for 1.60-1.66 Å).

1.2.4 Structural analysis and refinement

Structure analysis was carried out by molecular replacement method. We used *E. prolifera* plastocyanin with a 85% homology to *U. pertusa* plastocyanin as a search model. The amino acid sequence of *U. pertusa* plastocyanin is identical to *Ulva arasakii* plastocyanin (Yoshizaki *et al.*, 1989) except for residue 12 (correspond to residue 11 of poplar plastocyanin): Ala12 in *U. arasakii* plastocyanin is substituted to a serine in *U. pertusa* plastocyanin (Yoshizaki *et al.*, unpublished data). Fourteen nonidentical residues were replaced to an alanine. Rotation and translation searches were run using program *X-PLOR*. Diffraction data of 15.0-4.0 Å were used for these calculations. Patterson correlation refinement (Brünger, 1990) indicates that the seventh peak of the rotation function (θ_1=313.1˚, θ_2=46.4˚, θ_3=239.5˚) is the correct solution. Translation searches were carried out in space groups $P4_132$ and $P4_332$. A significant peak was obtained from the calculation with the space group $P4_332$ (x=0.759, y=0.315, z=0.111): The height of the top peak was T= 0.5731 for $P4_332$ and T= 0.2775 for $P4_132$. R-factor for 15.0-4.0 Å resolution shell was 0.44.

Amino acid residues were replaced by using program *TURBO-FRODO* (Roussel & Cambillau, 1989). A $2F_o - F_c$ electron density map clearly indicates the structures of the missing side chains. These side chains were fitted to the $2F_o - F_c$ electron density map. In the

first step of structural refinement, rigid-body refinement, positional refinement and individual temperature factor refinement were applied and the R_{work} decreased from 0.45 to 0.21 for 8.0-2.3 Å. In the third refinement step, thirty-nine water molecules were picked from an a F_o - F_c difference Fourier map. The R_{work} was decreased to 0.173 in this step. Gradually, resolution range was expanded and the 10.0-1.6 Å resolution data were included at the 15th step. Further three refinement steps gave the final model.

1.2.5 Overall structure and comparison with other plastocyanins

U. pertusa plastocyanin has the eight-stranded, antiparallel β-sandwich structure (Collyer *et al.*, 1990), which is identical to the plastocyanins from poplar, *C. reinhardtii* and *E. prolifera*. The β-sandwich can be divided into two β-sheets, β-sheet I and β-sheet II which are described by Freeman *et al.* (Collyer *et al.*, 1990). The β-sheet I consists of four β-strands; S1, residues 1-6; S2A, 14-15; S3, 26-31; S6 68-73 (Fig. 6). The β-sheet II also contains four β-strands; S2B, residues 18-22; S4, 39-40; S7, 78-83; S8 93-99. The copper site is located at northern end of the molecule (Fig. 6). Seven turns, turns 1-7, were found (Table III). The turn 2 is a type IVb turn (Richardson, 1981) with no hydrogen bond and bent at *cis*-Pro16. Two turns, the turn 3 and the turn 6 are type II turns and the others are type I turns. The turns 6 and 7 is located around the copper site. Hydrogen bonds in the backbones of the turns 6 and 7 are essential for maintaining the structure of the copper site.

Rms deviations of the structures between *U. pertusa*

plastocyanin and the others are as follows: poplar, 0.74 Å; *C. reinhardtii*, 0.62 Å; *E. prolifera*, 0.43 Å. Large deviations was found at four regions, around residues 26, 55, 70 and 87 (Fig. 7). The large deviation at the second region is due to the two inserted residues, 58 and 60, in poplar plastocyanin. The fourth region contains the turns 6 and 7, in which Cys84, His87 and Met92 construct a part of the copper site (Fig. 8). The structural difference of this site influences the structure of the copper site and we will discuss about it in the next section.

Fig.5 Crystal of plastocyanin.

Fig. 6 Schematic drawing of *U. pertusa* plastocyanin. Cu(II) and ligands are shown with ball-and-stick models at the top of the figure.

Fig. 7 Rms differences along the main-chain atoms (N, C_α, C, O) between the *U. pertusa* plastocyanin and the others, poplar (thin solid line), *C. reinhardtii* (thin broken line), and *E. prolifera* (thick solid line).

1.2.6 Comparison of the copper site with other plastocyanins and blue copper proteins

Cu(II) is coordinated by the four atoms, N_δ atoms of His37 and His87, S_γ atom of Cys84, and S_δ atom of Met92, in the distorted tetrahedral geometry (Fig. 8). The bond distances and the bond angles of the copper site are summarized in Table IV. The bond distance between Cu(II) and S_δ(Met92) is shorter by 0.13-0.23 Å than the other plastocyanins and is rather close to that of pseudoazurin and nitrite reductase (Table IV). This short Cu(II)-S_δ(Met92) distance can be explained by the structural differences at the turn 7 (residues 88-91). The large deviation is found at the turn 7 located around the copper site (Fig. 9). In this region, amino acid differences are found at only residue 85 and residue 88: *U. pertusa* has an alanine; *E. prolifera* has a serine; poplar and *C. reinhardtii* have a glutamine. The distance between C_α(residue 85) and Cα(residue 88) reveals the large deviation in the turn 7: *U. pertusa*, 5.43 Å; poplar, 5.36 Å; *C. reinhardtii*, 5.28 Å; *E. prolifera*, 5.07 Å. *E. prolifera* plastocyanin has the largest deviation from an average of the four structures and has the shortest distance between residue 85 and residue 88, due to a hydrogen bond between O(Asp85) and O_γ(Ser88), which withdraws the turn 7 to Asp85. Gln88 residues of poplar and *C. reinhardtii* plastocyanins have no hydrogen bond and have a weak interaction by stacking on an aromatic ring of Tyr83, which is the "remote site" residue. The distance between Asp85 and Gln88 may be shorten by this stacking interaction. *U. pertusa* plastocyanin without the interaction at the side chain of residue 88 has the largest distance between residue 85 and

residue 88.

The O(Asp85)-O_γ(Ser88) hydrogen bond pulls C_α(Met92) atom to Asp85 through the backbone of the turn 7 (Fig. 9). Compared with *U. pertusa* plastocyanin, Met92 rotates 12˚ with a fulcrum of its C_α atom, and C_α (Met92) atom translates by 0.4 Å. This effect lengthens the Cu(II)-S_δ(Met92) distance. Corresponding region of poplar and *C. reinhardtii* plastocyanin with a stacking interaction between Gln85 and Tyr83 is located at the intermediate state. In conclusion, the Cu(II)-S_δ(Met92) distance is strongly influenced by the structure of the turn 7: *U. pertusa* plastocyanin with the little restraint has the shortest distance of 2.69 Å, *E. prolifera* plastocyanin with the strong restraint has the longest distance of 2.92 Å, and poplar and *C. reinhardtii* plastocyanins with the weak restraint have intermediate distances of 2.82 Å and 2.89 Å, respectively.

Fig. 8 Ball-and-stick model at the copper site with a $2F_o - F_c$ electron density map. The map was contoured at a level of 1.5σ.

Fig. 9 Comparison of the structure of plastocyanins from *U. pertusa* (white), poplar (yellow), *C. reinhardtii* (orange), and *E. prolifera* (red), around the turn 7 and the copper site. Green dots mean the O_γ(Ser88)-O(Asp85) hydrogen bond in *E. prolifera* plastocyanin. This drawing is prepared by the program MidasPlus (Ferrin *et al.*, 1988; Huang *et al.*, 1991).

Ryde *et al.* calculated the energy of the copper site as a function of Cu(II)-S_δ(Met) distance (Ryde *et al.*, 1996). According to their result, the energies of the copper sites of *U. pertusa* and *E. prolifera* plastocyanins are higher by less than 1 kJ/mol and 5 kJ/mol respectively than the minimum energy point. The energy of the copper site of *E. prolifera* plastocyanin is then higher in less than 5 kJ/mol than that of *U. pertusa* plastocyanin if we consider only the Cu(II)-S_δ(Met) distance. The effect of the O(Asp85)-O_γ(Ser88) hydrogen bond in *E. prolifera* plastocyanin is redundant to cause the energy difference of the copper site if the effect of the hydrogen bond is taken to be 3 kcal/mol (correspond to 12.6 kJ/mol). The residual effect of the hydrogen bond (approximate 8 kJ/mol) may be partly absorbed by the turn 7 and the side chain of Met92 or the force of the hydrogen bond may be less than 3 kcal/mol. Thus, the shorter Cu(II)-S_δ(Met) distance caused by the O(Asp85)-O_γ(Ser88) hydrogen bond supports the results of the energy analysis on the Cu(II)-S_δ(Met) coordination.

In conclusion, *U. pertusa* plastocyanin, free from restraint by the hydrogen bond between residue 85 and residue 88, is close to the minimum energy state, whereas *E. prolifera* plastocyanin, with the elongated Cu(II)-S_δ(Met) bond by the O(Asp85)-O_γ(Ser88) hydrogen bond, has the higher energy state. This idea is also supported by facts that pseudoazurins from two species, *Alcaligenes faecalis* S-6 (Petratos *et al.*, 1988; Adman *et al.*, 1989) and *Methylobacterium extorquens* AM1 (Inoue *et al.*, 1994), have longer C_α(residue 79)-C_α(residue 82) distances, correspond to C_α(residue 85)-C_α(residue 88) in plastocyanin, than those of plastocyanins. Consequently, our crystal structure suggests that the Cu(II)-S_δ(Met) bond of *E. prolifera* plastocyanin is slightly

"racked" by the O(Asp85)-O_γ(Ser88) hydrogen bond.

U. pertusa plastocyanin has the longest Cu(II)-S_γ(Cys84) distance in all reported crystal structures of plastocyanins (Table III). This value is rather close to that of pseudoazurin and nitrite reductase than those of plastocyanins. The optimized Cu(II)-S_γ(Cys) distance (2.18 Å) (Ryde *et al.*, 1996) calculated by the quantum chemical theories is in good agreement with *U. pertusa* plastocyanin, pseudoazurin and nitrite reductase, whereas the other plastocyanins deviate significantly from the optimized distance; poplar, shorter in 0.11 Å; *E. prolifera*, shorter in 0.06 Å; *C. reinhardtii*, shorter in 0.07 Å (Table IV). The shorter Cu(II)-S_γ(Cys) distance is compensated by the longer Cu(II)-S_δ(Met) distance (Louis *et al.*, 1996). Therefore, the longer Cu(II)-S_γ(Cys) distance of *U. pertusa* plastocyanin may be due to the shorter Cu(II)-S_δ(Met) distance.

U. pertusa plastocyanin has the smallest positional differences of the ligated atoms between plastocyanins and pseudoazurin or between plastocyanins and nitrite reductase (Table V). This indicates that the copper geometry of *U. pertusa* plastocyanin is the closest to that of pseudoazurin and nitrite reductase, due to two reasons, the shorter Cu(II)-S_δ(Met92) and the longer Cu(II)-S_γ(Cys84) distance, and the coupled rotation of Cys84 and Met92 toward a square planer structure which increases the tetragonal Jahn-Teller distortion as described by Louis *et al.* (1996).

1.2.7 Structural Basis for Regulation of the Blue Copper Site by Residue 88

The present works firstly provide an experimental proof that the copper geometry is sensitive to the structure of the loop between His87 and Met92 (His-Met loop) (corresponding to turn 7 in *U. pertusa* plastocyanin). This means that the copper site of the blue-copper proteins is not so restrained as considered formerly (Vallee & Williams, 1968; Gray & Malmström, 1983; Malmström, 1994; Williams, 1995). However, it should be noted that the copper site is strained even if its effect is weak. Solomon and co-workers suggested that increased tetragonal distortion is due to the reduced rack or less entatic character (Louis *et al.*, 1996) This idea is consistent with our conclusion that *U. pertusa* plastocyanin with the increased tetragonal distortion is less restrained than the other plastocyanins.

In the case of azurin, another ligand of carbonyl oxygen coordinates with a distorted trigonal bipyramidal shape (Adman & Jensen, 1981; Baker, 1988; Nar *et al.*, 1991; Inoue *et al.*, 1994; Fraser *et al.*, 1995). Compared with the blue copper proteins with the distorted tetrahedral geometry, the Cu-S_δ(Met) distance is longer in approximate 0.3-0.5 Å. In azurin, the weak Cu-O bond attracts the copper ion to the ligated oxygen, lengthening the Cu-S_δ (Met). This is consistent with the soft interaction of the methioninyl sulfur with the copper ion and suggests that the Cu-O bond is well-balanced against the soft Cu-S_δ(Met) one in azurin.

It is impossible to control the copper geometry by the His-Met loop, if it were completely rigid. Flexibility of the copper site, especially Cu-S_δ(Met) bond, should be required. Consequently, the rack model (Malmström, 1983; Malmström, 1994; Williams, 1995), which agrees with the softness of the blue copper site, would

be more plausible for the blue copper proteins rather than the entatic theory (Vallee & Williams, 1968; Williams, 1995). The minimum rack energy, however, may be considerably lower than 70 kJ/mol reported by Malmström (Malmström, 1994). This means that intermolecular interactions can influence the structure of the blue copper site.

The copper geometry is crucial for the electron transfer ability, which indicates that the strength of the interaction between residue 85 and residue 88 which controls the Cu-S_{δ}(Met) geometry is quite important. In the His-Met loop, the discrepancy of primary structures from various sources is only found at residue 88 (Fig. 7), as described above. This implies that the conserved residues in the loop is essential to maintain its structure, whereas residue 88, probably, characterizes the properties of plastocyanin. The structural diverseness of the His-Met loop caused by the difference of residue 88 may vary the electron transfer rate in plastocyanin and other blue copper proteins.

Residue 88 which controls the structure of the His-Met loop is near Tyr83 which is in the negative or acidic patch and one of the electron transfer paths, as described above. The electron transfer reaction of plastocyanin with cytochrome *f* (He *et al.*, 1991) or P700 (Haehnel *et al.*, 1994) should occur when plastocyanin forms the complex with the negative patch (He *et al.*, 1991; Haehnel *et al.*, 1994). Residue 88 in the His-Met loop will then change its conformation by interacting with the pair, which will modify the geometry of the copper site through the loop. The complex should form the most appropriate conformation to reach the most efficient electron transfer reaction. Consequently, the geometry of the blue copper center may be transited into the most suitable form by the conformational transition of the loop.

In the Marcus theory (Marcus & Sutin, 1985), an electron transfer rate reaches its maximum value when the nuclear factor is optimized ($-\Delta G^{\circ} = \lambda$, where ΔG° and λ is the driving force and the reorganization energy, respectively). Moreover, the conformational transition is an important factor for the reorganization energy in a protein (Gray & Winkler, 1996). Within the complexes between plastocyanin and its pair, the most important conformational transition may occur probably at the His-Met loop and the copper site. That is to say, to reach the optimized condition of the nuclear factor, the conformational change of the His-Met loop occurs when the complex is formed, and then it may optimize the structure of the copper site.

1.2.8 Concluding remarks

The present study firstly reveals the structural basis for the cupric geometry regulated by the His-Met loop. This also shows the softness of the copper site. Furthermore, residue 88 in the His-Met loop seems to regulate the cupric geometry. However, the relationship between the type of residue 88 and the electron transfer rate remains unclear. Mutation studies at this position are necessary to clarify this and related questions. Finally, the present work provide an useful target to manipulate the copper-ligands geometry and the function of blue copper proteins with the site-directed mutagenesis.

1.3 References

Adman, E. T., Godden, J. W. & Turley, S. (1995). *J. Biol. Chem.*, **270**, 27458-27474.

Adman, E. T., Turley, S., Bramson, R., Petratos, K., Banner, D., Tsernoglou, D., Beppu, T. & Watanabe, H. (1989). *J. Biol. Chem.*, **264**, 87-99.

Badsberg, U., Jorgensen, A. M. M., Gesmar, H., Led, J. J., Hammerstad, J. M., Jespersen, L. L. & Ulstrup, J. (1996). *Biochemistry*, **35**, 7021-7031.

Bagby, S., Driscoll, P. C., Harvey, T. S. & Hill, H. A. (1994). *Biochemistry*, **33**, 6611-6622.

Brünger, A. T. (1990). *Acta Crystallog. sect. A*, **46**, 46-57.

Brünger, A. T. (1990). *Nature*, **355**, 472-475.

Church, W. B., Guss, J. M., Potter, J. J. & Freeman, H. C. (1986). *J. Biol. Chem.*, **261**, 234-237.

Collaborative Computational Project, Number 4 (1994). *Acta Crystallog. sect. D*, **50**, 760-763.

Collyer, C. A., Guss, J. M., Sugiyama, Y., Yoshizaki, F. & Freeman, H. C. (1990). *J. Mol. Biol.*, **211**, 617-632.

Colman, P. M., Freeman, H. C., Guss, J. M., Murata, M., Norris, V. A., Ramshaw, J. A. M. & Venkatappa, M. P. (1978). *Nature*, **272**, 319-324.

Cowtan, K (1994). *Joint CCP4 and ESF-EACBM Newsletter on Protein Crystallography*, 31, pp. 34-38.

Ferrin, T. E., Huang, C. C., Jarvis, L. E. & Langridge, R. (1988). *J. Mol. Graphics*, **6**, 13-37.

Gray, H. B., Malmström, B. G. (1983). *Comments Inorg. Chem.* **2**, 203-209.

Guss, J. M., Harrowell, P. R., Murata, M., Norris, V. A. & Freeman, H. C. (1986). *J. Mol. Biol.*, **192**, 361-387.

Guss, J. M., Bartunik, H. D. & Freeman, H. C. (1992). *Acta Crystallog. sect. B*, **48**, 790-811.

Hagler, A. T., Leiserowitz, L. & Tuval, M. (1976). *J. Am. Chem. Soc.*, **98**, 4600-4612.

Han, J., Adman, E. T., Beppu. T., Codd. R., Freeman, H. C., Huq, L. L., Loehr, T. M. & Sanders-Loehr, J. (1991). *Biochemistry*, **30**, 10904-10913.

Huang, C. C., Pettersen, T. E., Klein, T. E., Ferrin, T. E. & Langridge, R. (1991). *J. Mol. Graphics*, **9**, 230-236.

Higashi, T. (1989). *J. Appl. Cryst.* **22**, 9-18.

Inoue, T., Kai, Y., Harada, S., Kasai, N., Ohshiro, Y., Suzuki, S., Kohzuma, T. & Tobari, J. (1994). *Acta Crystallog. sect. D*, **50**, 317-328.

Kohzuma, T., Dennison, C., McFarlane, W., Nakashima, S., Kitagawa, T., Inoue, T., Kai, Y., Nishio, N., Shidara, S., Suzuki, S. & Sykes, A. G. (1995). *J. Biol. Chem.*, **270**, 25733-25738.

LaCroix, L. B., Shadle, S. E., Wang, Y., Averill, B. A., Hedman, B., Hodgson, K. O. & Solomon, E. I (1996). *J. Am. Chem. Soc.*, **118**, 7755-7768.

Malmström, B. G. (1994). *Eur. J. Biochem.*, **223**, 711-718.

Matthews, B. W. (1968). Solvent content of protein crystals. *J. Mol. Biol.*, **33**, 491-497.

Moore, J. M., Lepre, C. A., Gippert, G. P., Chazin, W. J., Case, D. A. & Wright, P. E. (1991). *J. Mol. Biol.*, **221**, 533-555.

Otwinowski, Z. (1993). *Data Collection and Processing. Proceedings of the CCP4 Study Weekend*, pp. 56-62. Warrington, England: Daresbury Laboratory.

Petratos, K., Dauter, Z. & Wilson, K. S. (1988). *Acta Crystallogr. sect. B*, **44**, 628-636.

Ramachandran, G. N., Kolaskar, A. S., Ramakrishnan, C. & Sasisekharan, V. (1974). *Biochim. Biophys. Acta*, **359**, 298-302.

Ramakrishnan, C. & Ramachandran, G. N. (1965). *Biophys. J.*, **5**, 909-933.

Redinbo, M. R., Cascio, D., Choukair, M. K., Rice, D., Merchant, S & Yeates, T. O. (1993). *Biochemistry*, **32**, 10560-10567.

Redinbo, M. R., Yeates, T. O. & Merchant, S. (1994). *J. Bioenerg. Biomembr.*, **26**, 49-66.

Richardson, J. S. (1981). *Advan. Protein Chem.*, **34**, 167-339.

Ryde, U., Olsson, M. H. M., Pierloot, K. & Roos, B. O. (1996). *J. Mol. Biol.*, **261**, 586-596.

Sakabe, N. (1991). *Nucl. Instrum. Methods Phys. Res.*, A**303**, 448-463.

Sato, M., Yamamoto, M., Imada, K., Katsube, Y., Tanaka, N. & Higashi, T. (1992). *J. Appl. Cryst.*, **25**, 348-357.

Solomon, E. I. & Lowery, M. D. (1993). *Science*, **259**, 1575-1581.

Takekuma, S., Takekuma, H., Matsubara, Y., Inaba, K. & Yoshida, Z. (1994). *J. Am. Chem. Soc.* **116**, 8849-8850.

Vallee, B. L. & Williams, R. J. P. (1968). M *Proc. Natl. Acad.*

Sci. USA, **59**, 498-505.

Williams, R. J. (1995). *Eur. J. Biochem.*, **234**, 363-381.

Yoshizaki, F., Fukazawa, T., Mishina, Y. & Sugimura, Y. (1989). *J. Biochem.* (Tokyo), **106**, 282-289.

2 Relationship between structure and enzymological properties of RuBisCO

2.1 Properties of RuBisCO

Ribulose-1,5-bisphosphate carboxylase/oxygenase (RuBisCO) is an enzyme that catalyzes primary reactions in photosynthesis as well as in photorespiration (Andrews & Lorimer, 1987). In the photosynthesis process, the enzyme catalyzes carboxylation reaction of ribulose-1,5-bisphosphate (RuBP), yielding two moles of 3-phosphoglycerate. The competing oxygenation reaction produces one mol of 3-phosphoglycerate and one mol of phosphoglycolate from RuBP. The oxygenation reaction reduces the rate of photosynthesis and severely limits crop yield. Consequently, the enhancement of carboxylation/oxygenation ratio is one of the most important factors for creating RuBisCOs with more useful properties for the current global problems.

The CO_2-fixation step catalyzed by RuBisCO in photosynthesis is the important rate-limiting step. RuBisCO of most photosynthetic organisms consists of eight large subunits (LS or *L*, 50-55 kDa) and eight small subunits (SS or *S*, 12-18 kDa). LS is the catalytic subunits but the function of SS is still unknown. The gene for LS locates in the plastid genome and that of SS in nuclei as a multigene family. The family gives rise to a few SSs with different primary structures. Yokota *et al.* have been studying the molecular and biochemical mechanisms of the evolution of the enzyme and its adaptation to the present oxygenic atmosphere after the appearance of the enzyme in the nature (Uemura *et al.*, 1996). It is known that RuBisCOs present at the present time still reflect the atmospheric conditions of the time when the enzymes began

to function in host organisms. For example, RuBisCO of higher land plants, which appeared after the atmosphere of the earth became oxygenic, has a higher affinity for CO_2 and a strong specificity for the carboxylase reaction than for the oxygenase reaction compared with the cyanobacterial enzyme, which appeared in a virtually an oxygenic but carbonated atmosphere. Inversely, plant RuBisCO has lost the ability to catalyze the reaction at high rates shown by photosynthetic bacterial and cyanobacterial enzymes. Another disadvantage of the plant enzyme is "fallover".

RuBisCO from plant sources loses its activity during the *in vitro* CO_2-fixation reaction to a stationary level (Yokota & Kitaoka, 1989; Robinson & Portis, 1989; Edmondson, Badger & Andrews, 1990; Zhu & Jensen, 1991). RuBisCOs from algae and photosynthetic bacteria hardly show such a loss of activity (Yokota & Kitaoka, 1989). The loss of the activity in the plant enzyme, "fallover", is composed of two components; hysteresis seen for the initial several minutes after the start of the reaction and the subsequent much slower decrease in activity. The latter loss is due to an accumulation of few suicide inhibitor formed from the substrate ribulose-1,5-bisphosphate (RuBP) at the catalytic site (Robinson & Portis, 1989; Edmondson, Badger & Andrews, 1990; Zhu & Jensen, 1991). I have found that two lysine residues Lys21 and Lys305 in the large subunits involved in the conformational change of the RuBisCO protein during hysteresis and are highly conserved among RuBisCOs from higher plants (Yokota & Tokai, 1993). The amino acid residues corresponding to these sites in the plant enzymes are changed into other residues in the algal and photosynthetic bacterial enzymes. The previous study with a fluorescent probe has revealed that binding of the intermediate analogue 2-carboxyarabinitol-1,5-bisphosphate (CABP) to the

catalytic sites of activated spinach RuBisCO induces a similar conformational change to that observed in hysteresis during the RuBP carboxylation (Yokota, 1991). The present study analyzed the protein structure near these lysine residues in the CABP-carbamylated spinach RuBisCO complex using the coordinates obtained at 1.8 Å resolution. The structure was compared with those of the carbamylated spinach enzyme (Taylor, Brändén, & Andersson, 1996) the carbamylated cyanobacterial enzyme-suicide inhibitor complex (Newman, Brändén, & Jones, 1993; Newman & Gutteridge, 1993).

Crystal structures of this L_8S_8 type RuBisCO were reported for two higher plants of tobacco (Chapman *et al.*, 1987; Chapman *et al.*, 1988; Curmi *et al.*, 1992; Schreuder *et al.*, 1993) and spinach (Knight, Andersson & Brändén, 1989; Knight, Andersson & Brändén, 1990; Taylor, Brändén, & Andersson, 1996; Andersson, 1996), and a cyanobacterium *Synechococcus* (Newman, Brändén, & Jones, 1993; Newman & Gutteridge, 1993). The rate of carboxylation and the affinity to the substrates are quite different between higher plants and cyanobacterium (Newman, Brändén, & Jones, 1993; Newman & Gutteridge, 1993). Nevertheless no significant structural difference of RuBisCO was found at the active site (Newman & Gutteridge, 1993), probably due to the conservation of the amino acid sequence around the active site.

Red algae RuBisCOs have higher substrate specificity factor ($V_{CO_2}K_{O_2}/V_{O_2}K_{CO_2}$) (Read & Tabita, 1994; Uemura *et al.*, 1996) than higher plants, green algae, and bacteria (Andrews, 1987; Uemura *et al.*, 1996). The gene sequences of red algal RuBisCOs (Valentin & Zetsche, 1989; Kostrzewa *et al.*, 1990; Valentin & Zetsche, 1990) indicate that the amino acid sequences around the active site are rather different from those of RuBisCOs obtained from other

species. In order to determine the reason for the high specificity factor, structural studies, especially at the active site, are essential.

2.2 Crystallization of RuBisCO

Crystals of spinach RuBisCO were grown by vapor diffusion with 6 ml drops containing a protein solution (15 mg/ml) in 7% polyethylene glycol 4000, 20 mM $MgCl_2$, 20 mM $NaHCO_3$, 1 mM dithiothreitol (DTT), 2 mM 2-carboxyarabinitol-1,5-bisphosphate (CABP), 50 mM Bicine (pH 7.9), and reservoir solutions containing 9% PEG4000, 20 mM $MgCl_2$, 20 mM $NaHCO_3$, 1 mM DTT, and 50 mM Bicine (pH7.9) at 298 K. Cell constants and a space group are determined by precession photographs. Crystals were of space group $C222_1$ with unit cell dimensions $a = 157.8$, $b = 157.8$, and $c = 200.9$ Å, isomorphous to crystals prepared with ammonium sulfate (Andersson & Brändén, 1984). If we assume that there are four large subunits and four small subunits in an asymmetric unit, the solvent content of the crystal is 46% (Vm = 2.27 Å^3/Da) (Matthews, 1968).

Galdieria RuBisCO was crystallized by the hanging drop vapor diffusion technique. Three microliters of a protein solution comprising 20 mM $MgCl_2$, 20 mM $NaHCO_3$, and 2 mM CABP was mixed with the same volume of the precipitant solution on a cover slide glass which was placed over a reservoir well containing precipitant solution. The droplet and the reservoir well was stored at 298 K. Crystallization conditions are listed in Table VI.

X-ray diffraction studies were carried out at room temperature with a Rigaku R-AXIS IIC imaging plate detector system mounted on a Rigaku RU-300 rotating-anode X-ray generator with a graphite monochromator (fine-focused Cu$K\alpha$, operating at 40kV and 100 mA). The crystal-to-detector distance was set at 160 mm and exposure time for each frame was 1 h. Each crystal was sealed in a thin-walled glass capillary. Cell constants were determined by means of the

auto-indexing routine of program, *DENZO* (Otwinowski, 1993). Data processing was carried out by with the program *DENZO* and *SCALEPACK*.

The crystallographic data are summarized in Table V. Two crystal forms were obtained: Form I crystal grew as a prismatic rod, and Form II ones as square plates. Both forms of crystal were grown by using polyethylene glycol 8000 as the precipitant. Form I crystal appeared after two months under low ion strength condition, while Form II ones grew completely within three days at higher ion strength than that for Form I. Only the Form I crystal was suitable for X-ray work. X-ray diffraction from the Form II crystal was too weak to determine its crystal data.

Intensity data were collected for a Form I crystal. Ninety frames with a rotation angle of 2.0˚ were recorded and processed. The combined set was obtained from 307,530 reflections in total, which were reduced to 82,842 unique reflections with an R_{merge} of 11.1% and a completeness of 86% to 3.0 Å resolution. The R_{merge} value is rather high because of the weak diffractions around 3.0 Å resolution and gradual X-ray damage to the crystal.

2.3 Data collection and structural refinement of spinach RuBisCO

Diffraction data from the spinach RuBisCO crystals were collected at room temperature with a Weissenberg camera for macromolecules (Sakabe, 1991) at the Photon Factory. A total of 586,168 observations was recorded from two crystals and was reduced to 216,085 unique reflections. The data were 67% complete to 1.6 Å resolution with an R_{merge} = 7.5%.

The crystal structure to 2.4 Å resolution of spinach RuBisCO was used as an initial model (Brookhaven Protein Data Bank ID code; 8RUB) (Knight, Andersson & Brändén, 1990). After rigid-body and positional refinement, simulated annealing method (Brünger, Kuriyan & Karplus, 1987) was used on SGI indigo2 and NEC EWS4800 workstations. Data between 6.0 and 2.5 Å were used for these calculations. After positional refinement and individual temperature factor refinement, an atomic model was fitted to a $2F_o - F_c$ electron density map with the program *FRODO* (Jones, 1985). Noncrystallographic restraints within the four LSs (L1, L2, L3, and L4) and the four SSs (S1, S2, S3, and S4) were used throughout the refinement process. Gradual expansion of the resolution range gave the final model.

2.4 Description of overall and active site structure of RuBisCO

The L_8S_8 RuBisCO is divided into four L_2 dimer composed of two LSs and eight SSs (Fig. 10). The LS of spinach RuBisCO consists of N-terminal domain built up from residues 1 to 150 and C-terminal domain composed of residues 151 to 475 (Fig. 11). The C-terminal domain has the α/β barrel motif with eight α-helices and eight β-strands. The catalytic center is comprised of the catalytic site of α/β barrel in the C-terminal domain of one LS and residues 60, 65, and 123 from the N-terminal domain of the neighboring LS in a L_2 dimer.

The structure at the active site is shown in Fig. 12. The Mg^{2+} is coordinated by six ligands, carbamylated Lys201, Asp203, Glu204, and two hydroxyl groups (O2 and O3) and a carboxyl group which corresponds to a fixed CO_2 in the CABP. Lys177, and Lys334 in loop 6 (Knight, Andersson & Brändén, 1990) form salt bridges with the carboxyl group in the CABP. These lysine residues should influence the charge distribution around CO_2 fixing site on RuBP, which implies that they are crucial for an activation energy and rate of CO_2 fixing.

The loop 6 in the C-terminal domain covers on the active site, which must stabilize the transit state. Furthermore, a C-terminal strand are fixed on the loop 6 in the CABP-carbamylated form. In the carbamylated form, the loop 6 and the C-terminal strand are free in order to introduce a RuBP into the active site (Taylor & Andersson, 1996).

Fig. 10 Space-fill model of L_8S_8 type RuBisCO. White and cyan models indicate the LSs, and blue one is the SSs.

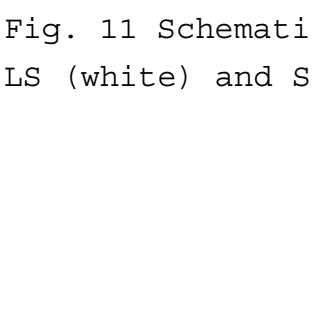

Fig. 11 Schematic drawing of LS (white) and SS (black)

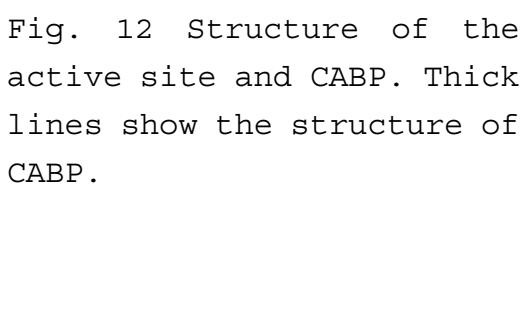

Fig. 12 Structure of the active site and CABP. Thick lines show the structure of CABP.

2.5 Structure of fallover sites

Yokota have reported that two lysine residues, Lys21 and Lys305, induce the hysteretic conformational change (Yokota & Tokai, 1993). Lys21 is found in the N-terminal domain and is 12 Å apart from the active site (Fig. 13). Lys305 faces the cleft formed between N-terminal and C-terminal domains of spinach RuBisCO.

In the carbamylated spinach RuBisCO, the side chain of Lys21 is free (Fig. 14). The carboxyl group of Glu60 forms hydrogen bonds with the OH group of Tyr20 and the amide group of Asn123 of the same N-terminal domain. One of the carboxyl oxygen of Glu52 makes hydrogen bonds with the peptidyl N of the same residue and the other is free. Large structural changes of spinach RuBisCO after binding CABP to the carbamylated form have spinach have been reported (Taylor & Andersson, 1996). α-Helix B comprised of the amino acid residues 50 to 60 and the N-terminal Asp19 to Lys21 are pulled than more 2 Å toward the catalytic center in the quaternary complex. The peptidyl O of Tyr20 and the peptidyl N of Lys21 form hydrogen bonds with the carboxyl oxygen of Glu52 in the complex. The carboxyl oxygen of Glu60 makes a hydrogen bond with the OH group of Tyr20 and a salt bridge with the amino group of Lys334 in loop 6 from the neighboring LS in a L_2 dimer. The amide group of Asn123 interacts with the carboxyl group of CABP on the catalytic site of the neighboring LS. Thus, the most sliding α-helix B is tied at the front and the end of the helix by the N-terminal residues in the quaternary complex.

Fig. 13 Locations of Lys21 and Lys305 at the fallover sites.

Fig. 14 Comparison of the structures around Lys21 and the active site between carbamylated RuBisCO (cyan) and carbamylated-CABP one (blue).

The ε-amino group of Lys21 forms a salt bridge with the carboxyl carbon of Asp19 in four of eight LSs of a holoenzyme (Fig. 16a). The group is free in the remaining four LSs (Fig. 16b). The two

structures of the side chain were due to a rotation of the chain between C_γ and C_δ. Considering the proposed structural function of the carboxyl group of Glu60 with the ε-amino group of Lys334, the distance between the ionic groups of these residues with influence the frequency of covering the site by the loop, namely the turnover rate in catalysis. The OE1 and OE2 of Glu60 are apart 3.05 and 3.12 Å from the NZ of Lys334 in spinach RuBisCO; the distance was 3.07 Å for both links in the cyanobacterial enzyme. The very slight difference in the distance may be important for a change in enzymatic properties between two RuBisCOs without any complete loss in activity, as has been discusses (Spreitzer, Thow & Zhu, 1995). The interactions between α-helix B and Tyr20 and Lys21 through Glu52 and Glu60 may influence the location of the carboxyl group of Glu60 in the catalytic site, namely the turnover rate. Furthermore, the location of Glu60 may be varied between two types of LS with or without the ionic interaction between the carboxyl group of Asp19 and the amino group of Lys21.

The side chain of Lys305 in the C-terminal domain forms ionic bonds with the carboxyl groups from Glu93 and Glu96 in the N-terminal domain of the same LS in the carbamylated form of spinach RuBisCO. The ε-amino group of Lys305 forms an ionic bond with the OE2 of Glu93 in four of eight LSs in the CABP-carbamylated RuBisCO quaternary complex; this state is called "K-E state", here (Fig. 16a). The side chain of Lys305 in the remaining four LSs is rotated between C_β and C_γ of the Lys305 to form an ionic bond with the C-terminal carboxyl carbon of Val475 of the same large subunit; this form is designated as "K-OXT state" (Fig. 16b). The N-terminal domain rotates 2˚ toward the catalytic site of the neighboring LS in the quaternary complex, and this rotation is the driving

force for the large movement of α-helix B toward the catalytic center to construct the catalytic center (Fig. 17). Thus, Lys305 may differently influence the rotation flexibility between the two states. The finding that removal of Val475 severely harms the catalysis in spinach RuBisCO (Portis, 1990) is well explained by the present observations. Lys305 is substituted by arginine in cyanobacterial RuBisCO which shows no hysteresis (Yokota, 1991; Yokota & Tokai, 1993). The guanidinyl group of Arg305 forms ionic bonds with the carboxyl group of Glu93 and the C-terminal carboxyl group at the same time in one LS (Fig. 16c).

a b

Fig. 15 Comparison of the structures of Lys21. a, L1 subunit, and b, L2 subunit.

Fig. 17 Comparison of the domain structure between carbamylated (thin lines) and its complex with CABP (thick lines)

a b c

Fig. 16 Ball-and-stick models of K-E state (a), K-OXT state (b), and corresponding site in *Synechococcus* RuBisCO (c).

2.6 Increment of water molecules during hysteretic structural change

Another observed large structural difference between the carbamylated form and the quaternary complex of spinach RuBisCO was the number of the water molecule bound to the enzyme. There are 1736 water molecules in the carbamylated form. The number of the molecule increased to 2412 in the quaternary complex. The increased number of the molecule locates mainly around the α-helix B/Asp19-Lys21 structure, between the C-terminal strand (residues 463 to 475) and loop 6, and in the cleft formed between N-terminal and C-terminal domains (Fig. 18). All of these regions are composed of the lysine residues involved in the hysteretic conformational change of RuBisCO as above. This observation is consistent with the previous results that the hydrophobic fluorescent probe attached to the carbamylated enzyme is kicked out of the enzyme protein during the hysteretic conformational change after binding of CABP, RuBP or 6-phosphogluconate to the catalytic sites (Yokota, 1991). Because the probe cannot re-attach the enzyme once it is released, the water molecules and two lysine enzyme once it is released, the water molecules and two lysine residues including α-helix B must be stabilized as they are in the quaternary complex, in contrast to loop 6. RuBisCO of a green alga *Euglena gracilis* possesses arginines at both positions and shows neither hysteresis nor release of the fluorescence probe during the reaction (Yokota, 1991). These considerations suggest that the slow movement of α-helix B to the catalytic site in the neighboring LS and the accompanying slow binding of water molecules to these and other regions are the molecular mechanism of hysteresis of spinach RuBisCO.

Fig. 18 Water molecules bound to RuBisCO. Red and yellow dots indicate the waters in the carbamylated and its complex with CABP, respectively. A stick model colored in orange shows CABP.

2.7 The plausible mechanism for the hysteretic structural change

The present structural studies indicate that Lys21 and Lys305 are key residues to introduce hysteresis into RuBisCO. Lys305 attracts the N-terminal domain through the K-E interaction (Fig. 19 A) as α-helix B keeps an "open" state in the carbamylated enzyme (Taylor & Andersson, 1996). This idea is strongly supported by the fact that *Rhodospirillum rubrum* RuBisCO without hysteresis reveals no domain rotation and α-helix B keeps closed state (Lundquvist & Shneider, 1989) and that Lys305 in unliganded and carbamylated spinach RuBisCO has the K-E interaction. On the contrary, Lys21 does not influence the domain rotation and the position of α-helix B because residues 1-19 are free and Lys21 forms no K-D state. C-terminal region of LS (residues 463-475) and loop 6 are also free. Binding of RuBP to the catalytic site initiates the reaction (Fig. 19 B). Loop 6 adopts a "closed" state to cover the transit state compound in the site for every turnover. The distance between the amino group of Lys334 in the closed state and the oxygen atoms of the carboxyl group of Glu60 in the open state is 5.2 and 5.8 Å, if other structures are the same. Since the amide nitrogen of Asn123 changes its direction from the carboxyl group of Glu60 to 2-carboxyl oxygen of the transit state compound for stabilizing the CO_2 fixed on RuBP (Fig. 12 & 14), the carboxyl oxygens may get much closer position to the amino group of Lys334. The N- and C-terminal regions of LS becomes to be fixed, and then Lys21 constructs the K-D interaction with Asp19, while K-E interaction of Lys305 may be broken to form the K-OXT state with the C-terminal carboxyl group (Fig. 19 C). The K-D interaction attracts the N-terminal domain to the catalytic site and α-helix

B occupied the closed state as depicted in Fig. 11. This transition state structure may give rise to a high activity before the hysteresis without any binding of the extra water molecules (Yokota, 1991). The closed form is stabilized by additional hydrogen bond networks formed by enclosed water molecules and peptides around the fixed N- and C-terminal regions and in the cleft between N- and C-terminal domains as discussed above (Fig. 19 D). The additional binding of water molecules must be quite slow because the fluorescent probe is released for a few minutes (Yokota, 1991). The stabilized closed form transits to the open state slowly (Fig. 19 G) since a half-life of the closed one is a few minutes (Yokota, 1991).

Fig. 19 The plausible mechanism for the hysteresis.

2.8 Orderly disposition of heterogeneous small subunits in RuBisCO from spinach

2.2.1 Multigene family of small subunits

Cells of green plants contain 50 to 100 chloroplasts, each of which has 20 to 900 copies of the genome (Mullet, 1988). Because of these large numbers, cells can synthesize much enzyme rapidly. The gene for LS is encoded in the plastid genome and 4 to 13 SS genes compose the multigene family in higher plants (Manzara & Gruissem, 1988). There being a multigene family of SS in plants probably facilitates fine tuning of the rate of synthesis of these subunits relative to LS (Dean, Dunsmuir & Bedbrook, 1987). All SS genes are expressed in green leaves of plants. The multiplicity in the genome construction may make possible transitory, organ-specific or signal-specific expression of different genes that have individual promoters (Meier *et al.*, 1995). Where do the translations of this multigene family in green leaves reside in the structure of RuBisCO holoenzyme? Crystal structures of RuBisCOs from tobacco (Chapman *et al.*, 1987; Chapman *et al.*, 1988; Curmi *et al.*, 1992; Schreuder *et al.*, 1993), spinach (Knight, Andersson & Brändén, 1989; Knight, Andersson & Brändén, 1990; Taylor, Brändén, & Andersson, 1996; Andersson, 1996), and a cyanobacterium (Newman, Brändén, & Jones, 1993; Newman & Gutteridge, 1993; Newman & Gutteridge, 1994) are consistent with a hexadecameric L_8S_8 structure in which all SSs are identical.

2.2.2 Structural heterogeneity in small subunits

The results of the structure analysis of the four pairs of an LS with an SS in an asymmetric unit of the crystal lattice are described above. While refining the structures, we found that the side chain skeletons of some residues in the SSs, reported by Martin (Martin, 1979), deviate significantly from our electron density maps, especially at residue 56, and that the shapes of the maps of the four crystallographically independent small subunits, named as *S*1, *S*2, *S*3, and *S*4, were different. Examination of the electron density maps suggested that residue 56 in *S*1 and *S*3 was leucine instead of the aspartate reported elsewhere (Martin, 1979), and that residue 56 in *S*2 and *S*4 was histidine (Fig. 20). The electron density maps at residue 93 suggested further structural differences; the reported alanine side chains of *S*2 and *S*4 fit the maps well, but *S*1 and *S*3 had a much longer side chain at this position (the residue could not be identified). Still other differences were observed in residue 8. These findings are evidence that spinach RuBisCO had two SS chains. Two-dimensional electrophoresis showed two peptides of SS with one LS peptide as reported before (Ren, Salnikow & Vater, 1991). With the pI of LS taken to be 6.13, as calculated from the reported amino acid sequence (Zurawski *et al.*, 1981) with GENETYX-MAX, Ver. 8 (Software Development Co., Ltd.), the pI points of the two SS peptides were 6.10 and 6.42. The observed difference in the pI's was partly due to the residue at position 56 being leucine in one peptide and histidine in the other. This difference should give rise to a difference in the pI of 0.13. The larger difference (0.32) actually found might be explained by other differences in the amino acid residues at positions 8 and 93 or elsewhere;

these could not be identified in this study. Thus, the results of X-ray diffraction analysis showed that spinach RuBisCO had two kinds of small subunits: S^{I}, with Leu56, and S^{II}, with His56. Spinach RuBisCO, therefore, has a $L_8S^{I}_4S^{II}_4$ structure, not L_8S_8 as reported before (Knight, Andersson & Brändén, 1989; Knight, Andersson & Brändén, 1990; Taylor, Brändén, & Andersson, 1996; Andersson, 1996).

2.2.3 Symmetrical configuration of the small subunits and interactions between the large subunits and the small subunits

Figure 21 shows the $L_8S^{I}_4S^{II}_4$ structure schematically. Earlier spinach RuBisCO was described as having D_4 point symmetry (Knight, Andersson & Brändén, 1989; Knight, Andersson & Brändén, 1990; Taylor, Brändén, & Andersson, 1996; Andersson, 1996), which would be possible only if RuBisCO were composed of eight identical large subunits and eight identical small subunits. Our X-ray results showed that what might be the fourfold symmetry of spinach RuBisCO was broken by the heterogeneity of the SSs. The same kind of the small subunits occupies the positions furthest from each other, maintaining twofold symmetry along the central core.

The NE2 atom of His56 in the S^{II} subunits forms a hydrogen bond with the carbonyl oxygen atom of Glu259 in the neighboring large subunit (Fig. 20). On the other hand, the side chain of Leu56 of the S^{I} subunits does not interact electrostatically. The additional S^{II}His56NE2-LGlu259O hydrogen bond must cause the difference in the dissociation constants; the L-S^{II} interaction must be more stable because of the hydrogen bond between His56 and Glu259, and the S^{II} subunit will construct the L-S pair more

readily than S^{I}. In this context, it is interesting to recall the finding that a highly conserved sequence of 16 amino acids, including that at position 56, are essential for the assembly of LS and SS in the plant enzyme (Wasmann *et al.*, 1989).

In terms of its different interactions of the two SSs, *L* also may be of two kinds; the structure of spinach RuBisCO may be $\{(L^{I}/L^{I})_2S^{I}_4\}\{(L^{II}/L^{II})_2S^{II}_4\}$, where L^{II} is the *L* that has the S^{II}His56-^{L}Glu259 hydrogen bond and L^{I} does not have such a bond, L^{I}/L^{I} and L^{II}/L^{II} mean L_2 dimers (Andersson & Brändén, 1990) formed by same kind of large subunits. ^{L}Glu259 participates in a dimer-dimer interaction with ^{L}Arg258 in the neighboring L_2 dimer and may be involved in the transfer of signals of an L_2 dimer to the next one.

2.2.4 Relation between heterogeneity in the small subunit and regulatory sites

Plant RuBisCO gradually decreases in activity to a constant level during reaction (Yokota, 1991). The decrease is smaller if there is binding of the substrate ribulose-1,5-bisphosphate to the noncatalytic substrate-binding sites (Yokota, Wadano & Murayama, 1996). Binding of ribulose-1,5-bisphosphate to these sites proceeds cooperatively; binding to the first four sites suppresses binding to the remaining four sites (Yokota, Higashioka & Wadano, 1991; Yokota *et al.*, 1994). The grouping of eight large and eight small subunits into two different structures as described above may give an account for the cooperativity in plant RuBisCO. Thus, there being a multigene family for SS may be related to a genetic mechanism that has given the enzyme the ability to fine-tune its own catalysis.

Fig. 20. Ball-and-stick stereo models around residue 56 of four small subunits with $2F_o$ - F_c electron density maps: *a* , *S*1; *b*, *S*2; *c*, *S*3; and *d*, *S*4. The green broken lines in *b* and *d* show the ^{S}His56 NE2-^{L}Glu259 O hydrogen bonds. These density maps were calculated without the contribution of residue 56. The contour level of all maps is set at 1.5σ.

Fig. 21. Schematic drawing of the $L_8S^{I}_4S^{II}_4$ structure. The S^{I} and S^{II} subunits are shown as cyan and blue wire models respectively. The white dots show the Cα atoms of the eight large subunits. There are three twofold axes in the spinach RuBisCO molecule: one of them corresponds to a crystallographic axis (red) and the others are noncrystallographic axes (white). This drawing was prepared using MidasPlus (Ferrin *et al.*, 1988; Huang *et al.*, 1991).

2.3 References

Andersson, I. (1996). *J. Mol. Biol.* **259**, 160-174.

Andersson, I. & Brändén, C. -I. (1984). *J. Mol. Biol.* **172**, 363-366.

Andrews, T. J. & Lorimer, G. H. (1987). *The Biochemistry of Plants*, Vol. 10, 131-218, Academic Press, New York.

Brünger, A. T., Kuriyan, J. & Karplus, M. (1987). *Science* **235**, 458-460.

Chapman, M. S., Suh, S. W., Cascio, D., Smith, W. W. & Eisenberg, D. (1987). *Nature* **329,** 354-356.

Chapman, M. S., Suh, S. W., Curmi, P. M. G., Cascio, D., Smith, W. W. & Eisenberg, D. S. (1988). *Science* **241**, 71-74.

Curmi, P. M. G., Cascio, D., Sweet, R. M., Eisenberg, D. & Schreuder, H. (1992). *J. Biol. Chem.* **267**, 16980-16989.

Dean, C., Dunsmuir, P. & Bedbrook, J. (1987). *Tailoring Genes for Crop Improvement: An Agricultural Perspective* 59-68, Plenum Press, New York.

Edmondson, D. L., Badger, M. R., & Andrews, T. J. (1990). *Plant Physiol.*, **93**, 1390-1397.

Ferrin, T. E., Huang, C. C., Jarvis, L. E. & Langridge, R. (1988). *J. Mol. Graphics* **6**, 13-37.

Huang, C. C., Pettersen, T. E., Klein, T. E., Ferrin, T. E. & Langridge, R. (1991). *J. Mol. Graphics*, **9**, 230-236.

Johns, T. A. (1985). *Meth. Enzym.* **115**, 157-171.

Knight, S., Andersson, I., and Brändén, C. -I. (1989). *Science* **244**, 702-705.

Knight, S., Anderson, I., and Brändén C. -I. (1990). *J. Mol. Biol.* **215**, 113-160.

Kostrzewa, M., Valentin, K., Maid, U., Radetzky, R. and Zetsche, K. (1990). *Curr. Genet.* **18**, 465-469.

Lundquvist, T., & Shneider, G. (1989). *J. Biol. Chem.*, **264**, 7078-7083.

Manzara, T., and Gruissem, W. (1988). *Photosynth. Res.* **16**, 117-139.

Martin, P. G. (1979). *Aust. J. Plant Physiol.* **6**, 401-408.

Matthews, B. W. (1968) *J. Mol. Biol.* **33**, 491-497

Meier, I., Callan, K. L., Fleming, A. J., and Gruissem, W. (1995). *Plant Physiol.* **107**, 1105-1118.

Mullet, J. E. (1988). *Annu. Rev. Plant Physiol. Plant Mol. Biol.* **39**, 475-502.

Newman, J., and Gutteridge, S. (1993). *J. Biol. Chem.* **268**, 25876-25886.

Newman, J., Brändén, C. -I., and Jones, T. A. (1993). *Acta Crystallogr.* D**49**, 548-560.

Newman, J, & Gutteridge, S. (1993). *Structure*, **2**, 495-502.

Otwinowski, Z. (1993). *Data Collection and Processing. Proceedings of the CCP4 Study Weekend*, pp. 56-62. Warrington, England: Daresbury Laboratory.

Portis, Jr., A. R. (1990). *Arch. Biochem. Biophys.*, **283**, 397-400.

Read, B. A. and Tabita, F. R. (1994). *Arch. Biochem. Biophys.* **312**, 210-218.

Ren, L., Salnikow, J., and Vater, J. (1991) *Plant Sci.* **74**, 1-6.

Robinson, S. P., & Portis, Jr., A. R. (1989). *Plant Physiol.*, **90**, 968.

Sakabe, N. (1991). *Nucl. Instrum. Methods Phys. Res.*, A**303**, 448-463.

Schreuder, H. A., Knight, S., Curmi, P. M. G., Andersson, I. Cascio, D., Sweet, R. M., Brändén C. -I., and Eisenberg, D. (1993). *Protein Science* **2**, 1136-1146.

Spreitzer, R. J., Thow, G., & Zhu, G. (1995). *Plant Physiol.*, **109**, 681.

Taylor, T. C., and Andersson, I. (1996). *Nature Struct. Biol.* **3**, 95-101.

Uemura, K., Suzuki, Y., Shikanai, T., Wadano, A., Jensen., R. G., Chmara, W. and Yokota, A. (1996). *Plant Cell Physiol.* **37**, 325-331.

Valentin, K. and Zetsche, K. (1989). *Curr. Genet.* **16**, 203-209.

Valentin, K. and Zetsche, K. (1990). *Mol. Gen. Genet.* **222**, 425-430.

Wasmann, C. C., Ramage, R. T., Bohnert, H. J., and Ostrem, J. A. (1989). *Proc. Natl. Acad. Sci U.S.A.* **86**, 1198-1202.

Yokota, A., & Kitaoka, S. (1989). *Plant Cell Physiol.*, **30**, 183-191.

Yokota, A. (1991). *J. Biochem.* **110**, 246-252.

Yokota, A., Higashioka, M., and Wadano, A. (1991). *J. Biochem.* **110**, 253-256.

Yokota, A. & Tokai, H. (1993). *J. Biochem.* **114**, 746-753.

Yokota, A., Higashioka, M., Taira, T., Usuda, H., Wadano, A., and Murayama, H. (1994). *Plant Cell Phisiol.* **35**, 317-321.

Yokota, A., Wadano, A., and Murayama, H. (1996). *J. Biochem.* **119**, 487-499.

Zhu, G., & Jensen, R. G. (1991). *Plant Physiol.*, **97**, 1354-1358.

Zurawski, G., Perrot, B., Bottomley, W., and Whitfeld, P. R. (1981). *Nucleic Acids Res.* **9**, 3251-3270.

Conclusion

The present works should contribute the elucidation of the mechanism and the function of the photosynthesis. Chromoprotein realizes the novel photosynthetic reaction mechanism. The structural studies on the enzyme will clarify the roles of indolone. The crystal structure of chromoprotein was solved at 2.8 Å resolution by MIR method. Current electron density maps indicates that chromoprotein has elongated shape with six-bundled α-helices. The active site may be involved in these α-helices.

Ulva pertusa plastocyanin with the novel cupric geometry in plastocyanin suggests that the blue copper site is not as rigid as considered before. The present works show that the loop between His87 and Met92 control the coordination geometry of the copper site. The flexibility of Cu-Sδ(Met) bond may be important its redox activity.

This works also clarify the fallover mechanism of RuBisCO. Two lysine residues which induce hysteretic conformational change have two conformation and cause the domain rotation. This structural transition is accompanied by additional binding of waters into the enzyme. The present studies suggest that the hysteresis observed in higher plant RuBisCO is due to the structural changes and binding waters.

Two kinds of the small subunits was found in spinach RuBisCO in the orderly way. The half of the eight regulatory sites has the different affinity for the remaining sites. The heterogeneity of SSs may regulate the activity of RuBisCO.

List of Publications

(1) Orderly Disposition of Heterogeneous Small Subunits in D-Ribulose-1,5-Bisphosphate Carboxylase/Oxygenase from Spinach.
N. Shibata, T. Inoue, K. Fukuhara, Y. Nagara, R. Kitagawa, S. Harada, N. Kasai, K. Uemura, K. Kato, A. Yokota, and Y. Kai
J. Biol. Chem., **271**, 26449-26452 (1996)

(2) Crystallization and Preliminary Crystallographic Studies of Ribulose 1,5-Bisphosphate Carboxylase/Oxygenase from a Red Alga, *Galdieria partita*, with a High Specificity Factor.
N. Shibata, H. Yamamoto, T. Inoue, K. Uemura, A. Yokota, and Y. Kai
J. Biochem., **120**, 1064-1066 (1996)

(3) Crystallization and Preliminary Crystallographic Studies of Pink Color Chromoprotein from *Pleurotus salmoneostramineus* L. Vass..
N. Shibata, M. Gohow, T. Inoue, C. Nagano, K. Inaba, H. Takekuma, S. Takekuma, Z. Yoshida, and Y. Kai
Acta. Cryst. sect. D, in press

(4) Structure of Azurin from *Achromobacter xylosoxidans* NCIB11015 at 2.5 Å Resolution.
T. Inoue, N. Shibata, H. Nakanishi, S. Koyama, H. Ishii, Y. Kai, S. Harada, N. Kasai, Y. Ohshiro, S. Suzuki, T. Kohzuma, K. Yamaguchi, S. Shidara, and H. Iwasaki
J. Biochem. **116**, 1193-1197 (1994)

(5) Novel Insight into the Copper-Ligands Geometry in the Crystal Structure of *Ulva pertusa* Plastocyanin at 1.6 Å resolution.
N. Shibata, T. Inoue, N. Nishio, C. Nagano, T. Kohzuma, K. Onodera, F. Yoshizaki, Y. Sugimura, and Y. Kai
Submitted to *J. Mol. Biol.*

(6) Structural and Enzymological Analysis of Two Hysteretic Lysine Residues in RuBisCO.
in preparation

Acknowledgment

The author is particularly grateful to professor Yasushi Kai for his constant guidance, supporting the present studies, and his hospitality. The author express gratitude to emeritus professor Nobutami Kasai for his helpful suggestions and hearty encouragement. The author wishes to thank Dr. Shigeharu Harada for his useful and hearty advice. The author acknowledges to Dr. Tsuyoshi Inoue for his useful suggestions and guidance. The author also acknowledge to Dr. Nobuko Kanehisa and Mrs. Eiko Mochizuki for their suggestions and hearty supports.

The author is certainly indebted to professor Akiho Yokota for his advice and suggestions about the structural and enzymological studies of RuBisCO. The author acknowledges to professor Shinnichiro Suzuki for his useful advice for the studies on metalloproteins and in purification of proteins. He also acknowledges to emeritus professor Zen-ichi Yoshida for his useful suggestions about chromoprotein. The author greatly thanks Dr. Takamitsu Kohzuma and Dr. Kazuya Yamaguchi for his helpful advice and suggestions about metalloproteins and in purification of proteins. He also greatly thanks Dr. Shin-ichi Takekuma and Dr. Hideko Takekuma for their useful advice for studies on chromoprotein. The author acknowledges to Mr. Koichi Uemura and Dr. Ko Kato for their useful advice and helps for studies on RuBisCO. He also acknowledges to Mrs. Naomi Nagasawa for her kind helps in preparing figures and discussions on RuBisCO.

The author wishes to thank professor Noriyoshi Sakabe, Dr. Atsushi Nakagawa, Dr. Nobuhisa Watanabe, and Dr. Mamoru Suzuki for their helpful advice and supporting data collection at KEK.

The author acknowledges to Dr. Susumu Yoshikawa and Dr. Hitoshi

Yamamoto for their kind advice and supporting the data collection at Osaka National Research Institute.

The author is grateful to Mr. Ryouichi Kitagawa, Mr. Kazuhiro Fukuhara, Miss Chizuko Nagano, Mr. Yoshitaka Nagara, Mr. Manabu Gohow, and Mr. Hiroki Yamamoto for their collaborations, and all members in his laboratory for their helpful suggestions and cooperation.

Finally, I wish to thank my parents for their constant and helpful supports.